Journal of Power Sources 205 (2012) 367–376

Contents lists available at SciVerse ScienceDirect

Journal of Power Sources

journal homepage: www.elsevier.com/locate/jpowsour

A micro-reactor with micro-pin-fin arrays for hydrogen production via methanol steam reforming

Deqing Mei[a,*], Miao Qian[a], Binhong Liu[b], Biao Jin[a], Zhehe Yao[a], Zichen Chen[a]

[a] The State Key Lab of Fluid Power Transmission and Control, Department of Mechanical Engineering, Zhejiang University, Hangzhou, Zhejiang 310027, PR China
[b] Department of Material Science and Engineering, Zhejiang University, Hangzhou, Zhejiang 310027, PR China

ARTICLE INFO

Article history:
Received 28 October 2011
Received in revised form
14 December 2011
Accepted 20 December 2011
Available online 12 January 2012

Keywords:
Micro-reactor
Micro-pin-fin arrays
Hydrogen production
Methanol steam reforming
Numerical analysis

ABSTRACT

To enhance the compactness of the micro-reactors for hydrogen production via methanol steam reforming (SMR) for fuel cell, a novel micro-reactor with micro-pin-fin arrays (MPFAR) is designed and fabricated based on the micro thixo-forming technology. A three-dimensional model is adopted in the numerical analysis to investigate the heat and mass transfer in the micro-reactor. The results show that the methanol conversion in the MPFAR is higher than that in a micro-channel reactor, the velocity and temperature distribution is uniform in the catalyst support. Higher reaction temperature and contact time result in higher methanol conversion and CO molar fraction at the outlet, while a higher steam to methanol ($S\,C^{-1}$) molar ratio results in a lower CO molar fraction. Finally, experiments are conducted to test the performance of the MPFAR for hydrogen production. The experimental results agree well with the simulated ones, which validate the accuracy of the simulation model. When the $S\,C^{-1}$ molar ratio and the contact time are 1.2 and 0.12 s, respectively, the methanol conversion of the MPFAR reaches to 87.5% with the hydrogen molar fraction of about 75% at the outlet, which is suitable for the application in the fuel cell system.

1. Introduction

The fuel cell vehicles present several advantages compared with the internal combustion engine vehicles including less CO_2 emission and less energy cost [1]. Also, the hydrogen energy adopted in the fuel cell vehicles has high energy density and little impact on surroundings, while the fossil fuel destroys environment and will exhaust in the near future [2]. However, a major challenge for the commercialization of the fuel cell vehicles is the hydrogen supply. An available approach [3] to overcome this challenge is developing a compact fuel processor to produce hydrogen on board by reforming reactions, such as methanol [7], alcohol [4–6] and so on. Among these methods for hydrogen production, on-board methanol steam reforming has attracted significant interest because of its low reaction temperature, good miscibility with water, high hydrogen concentration and lower carbon monoxide concentration in the reformate gas [8].

To obtain high-performance on-board methanol steam reforming system, several types of reactors have been proposed and studied in recent years. Kolb et al. [9] have revealed that the plate reactors have better performance than the cylindrical reactors due to the intensification of the heat and mass transfer. Among all kinds of plate reactors for hydrogen production, the micro-channel reactors provide higher specific surface area, heat and mass transfer rate and controllability [10]. Therefore, the micro-channel reactors for hydrogen production via methanol steam reforming have received increasing attentions from the academic community all over the world. Park et al. [11] have developed a micro-channel methanol steam reformer with the dimension of about 70 mm × 40 mm × 30 mm, which could generate adequate hydrogen for a 15 W fuel cell. Kunda et al. [12] have proposed a MEMS-based micro-fuel processor, and found that the serpentine channeled micro-reformer has better performance than the parallel channeled one for hydrogen production. Zhou et al. [13] have fabricated a novel micro-channel reactor using porous copper fiber sintered felt as the catalyst support. The new catalyst support used in their micro-channel reactor enhanced the adhesion of catalyst, improved the catalyst life and increased the methanol conversion.

For thoroughly examining the performances of the reactor, many experiments need to be carried out, which are very time-consuming. Consequently, modeling and numerical studies are usually adopted to get a deep understanding of the heat and mass transfer in a micro-channel reactor for hydrogen production via methanol steam reforming. During the past decades, many numerical models have been used in the analysis, including one-dimensional models [14–16], two-dimensional models [17–21] and three-dimensional models [22,23]. The mass and heat balance equations have been adopted by Kawamura et al. [14] to design

* Corresponding author. Tel.: +86 571 8795 1906; fax: +86 571 8795 1145.
E-mail address: medqmei@zju.edu.cn (D. Mei).

0378-7753/$ – see front matter © 2012 Elsevier B.V. All rights reserved.
doi:10.1016/j.jpowsour.2011.12.062

Nomenclature

C_i	inlet molar concentration of methanol (mol m^{-3})
C_p	specific heat in constant pressure (J kg^{-1} K^{-1})
C_{out}	outlet molar concentration of methanol (mol m^{-3})
CH_3OH	methanol
CO	carbon monoxide
CO_2	carbon oxide
D	inlet (or outlet) tube internal diameter (m)
d	micro-pin-fin diameter (m)
H	micro-channel height (m)
H_2	hydrogen
H_2O	steam
h	micro-pin-fin arrays height (m)
k_1	rate constant of the steam reforming reaction
k_2	forward rate of the reverse water-gas shift reaction
k_{-2}	backward rate of the water-gas shift reaction
L	micro-channel length (m)
L_M	flow manifold length (m)
M_{CO}	molar fraction of carbon monoxide
M_i	molar fraction of species i
M_{ws}	molecular weight of the species s (g mol^{-1})
MPFAR	micro-reactor with micro-pin-fin arrays
p	pressure of fluid (Pa)
P_s	partial pressure of species s (Pa)
R_{rWGS}	reaction rate of the reverse water-gas shift reaction (mol m^{-3} s^{-1})
R_s	species source term for the reforming reaction (kg m^{-3} s^{-1})
R_{SR}	reaction rate of the steam reforming reaction (mol m^{-3} s^{-1})
R_r	energy source term for the reforming reaction
S_D	longitudinal center-to-center distance (m)
SMR	methanol steam reforming
S_T	transverse center-to-center distance (m)
SC^{-1}	steam to methanol
S_u, S_v, S_w	sources terms produced by the porous structure of catalyst
T	fluid temperature (K)
Tr	reaction temperature (K)
W	micro-channel width (m)
x, y, z	Cartesian coordinates (m)
u, v, w	velocity components in the x, y and z direction, respectively (m s^{-1})

Greek symbols

η	methanol conversion
κ	fluid heat conductivity (W m^{-1} K^{-1})
μ	dynamical viscosity (kg m^{-1} s^{-1})
ρ	density of fluid (kg m^{-3})
τ	contact time (s)
φ	fluid viscous dissipation term

a micro-channel reactor and successfully simulate the methanol conversion and the species concentration in the reformate gas. Suh et al. [19] have proposed a two-dimensional model to analyze the transport phenomena in a methanol steam reformer. The simulated results based on this model were found to agree well with the experimental results. They also found that higher methanol conversion and carbon monoxide concentration can be obtained with internal heating. Hsueh et al. [22] have used a three-dimensional model to study the effect of the geometrical structure and the thermo-fluid parameters on the methanol conversion and the efficiency of the micro-channel reformers. Their simulated results revealed that a low aspect-ratio micro-channel and a reasonable operation situation can enhance the performances of the micro-reformer. Hsueh et al. [23] have studied the performance of a plate methanol steam micro-reformer with serpentine flow field design using a three-dimension model. They found that the conduction through the wall has a crucial effect on the temperature distribution and needs to be considered in the analysis. They also found that the methanol conversion is higher with top plate heating than with base plate heating.

Although the structural designs and the models of the micro-channel reactors for hydrogen production have been widely studied, the high fabrication cost and the relatively low performance are still challenges regarding the commercialization of this technique. In this study, a micro-reactor with micro-pin-fin arrays (MPFAR) was designed to increase the energy density. The catalyst support of the micro-reactor was fabricated based on micro thixo-forming technology, which could significantly reduce the fabrication cost for mass production. To quantitatively analyze the catalytic performance of the micro-reactor for hydrogen production, the numerical studies were carried out for the heat and mass transfer through the micro-pin-fin arrays in the micro-reactor. In addition, experiments were conducted to test the performance of the micro-reactor and validate the accuracy of the numerical model.

2. Design and fabrication of the MPFAR

2.1. Design of the MPFAR

A novel MPFAR was proposed to enhance the compactness of the reactors, the structure of which is shown in Fig. 1. The larger surface area of the MPFAR than the plate-typed micro-channel reactor benefits the methanol steam reforming (SMR) reaction for hydrogen production. The micro-reactor is composed of a catalyst support, a chamber, a cover plate to connect with the inlet and outlet tubes and a heated plate. The catalyst support is a metal plate with cylindrical micro-pin-fin arrays, and the heights of the micro-pin-fins are uniform as well as the center-to-center distance between each two micro-pin-fins. The catalyst used for methanol steam reforming is coated on the catalyst support. The chamber is a metal plate with a rectangular groove for mounting the catalyst support and two right triangle flow manifolds for homogenizing the flow field. The heated plate is used to install the cartridge heaters for heating the micro-reactor, and the material of the heated plate is A356 to ensure that the material of the wall contacted with reagent is identical. The cover plate with a material of stainless steel is used to connect with inlet and outlet steel tubes, and the sealing method between them adopts the argon arc welding. The chamber with the catalyst support, the heated plate and the cover plate were stacked to compound the reactor. Graphite was used as the sealing material to seal the MPFAR attributed to its better heat resistant and ductility than the metal gaskets. The micro-reactor is heated by cartridge heaters inserted in the heated plate and the chamber. The reaction gas mixture goes into the MPFAR from the inlet and goes out from the outlet.

2.2. Fabrication of the catalyst support

Conventional machining was adopted to fabricate the reaction chamber. The manufacture of the catalyst support, which is the key portion of the micro-reactor, is difficult because of its size and complex topology structure. The conventional methods to fabricate the catalyst support are silicon bulk fabrication [24], ultra-precision machining [25], and LIGA process. However, the low productivity, high-cost and high energy consumption have hindered their wide application in micro-reactor fabrication. To overcome these

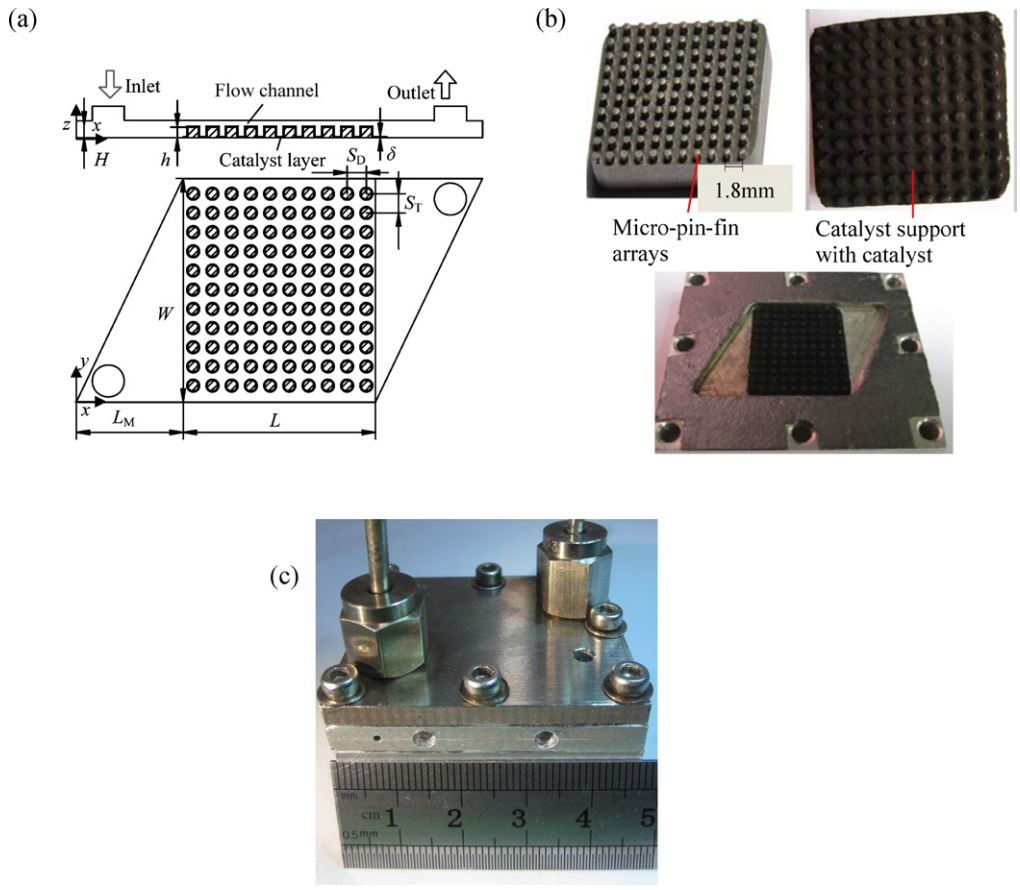

Fig. 1. Design of the MPFAR: (a) 2-D structure diagram; (b) fabricated catalyst support using micro thixo-forming process; (c) fabricated MPFAR.

obstacles, the semi-solid micro thixo-forming processing, which was proposed by Steinhoff et al. [26] and developed by Kim et al. [27,28], provided a low-cost and high-efficiency approach for the micro-reaction support with micro-pin-fin arrays. In this study, the semi-solid micro thixo-forming processing was adopted to fabricate the catalyst support with micro-pin-fin arrays, and its specific manufacture procedures were as follows.

Aluminum alloy A356 is used to fabricate the catalyst support attributed to its low density and good performance in semisolid forming. The fabrication apparatus and procedure of the MPFAR are shown in Fig. 2. Firstly, based on the material characteristic and the feature of the micro thixo-forming technology, the cylindrical workpiece was heated by the induction heating instrument. In order to obtain uniform temperature distribution in the workpiece in this study, by controlling the induction heating instrument, the workpiece was heated quickly at the beginning of the heating process, then heated slowly when the temperature of the workpiece approached to 853 K approximately, which is at the semi-solid range of A356 alloy as shown in Fig. 2(a). The detail introduction about the optimization of the heating process is addressed in the previous publication [29]. Then, the heated workpiece was moved quickly into the dies mounted on 100 kN mechanical press as shown in Fig. 2(b). The punch with micro-hole arrays machined by micro-milling was used to fabricate the micro-pin-fin arrays. The lower mould of the die has a chamber to place the heated workpiece. The dies were preheated to Ca. 500 K to improve the

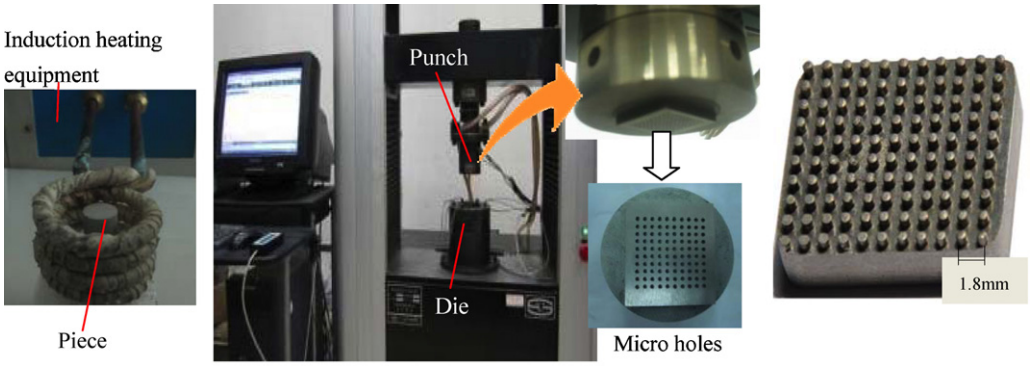

Fig. 2. Catalyst support fabrication process: (a) induction heating; (b) micro thixo-forming process; (c) fabricated catalyst support.

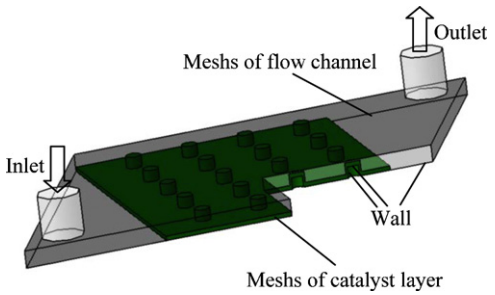

Fig. 3. The 3-D simulation model of the MPFAR.

process characteristic of the workpiece. Finally, the mechanical press moved down quickly to press the heated workpiece, and the catalyst support with micro-pin-fin arrays used in the micro-reactor for hydrogen production was well fabricated based on the micro thixo-forming technology as shown in Fig. 2(c).

3. Model development

In order to analyze the mass and heat transfer and the reaction performance in the MPFAR developed in this study, a three-dimensional simulation model was established. By adopting this three-dimensional simulation model, the performance of the MPFAR was analyzed in comparison with a micro-channel reactor. The results demonstrate that the MPFAR has better performance in producing hydrogen via SMR for fuel cell.

3.1. Model description

The structure diagram and the calculation domain of the MPFAR are shown in Figs. 1 and 3. The model consists of two sections: catalyst layer and flow channel. The catalyst layer is coated on catalyst support, and the flow channel is the rest except the catalyst layer. The detail structure parameters of the MPFAR are listed in Table 1. For comparison, a micro-channel reactor of 12 micro-channels was also analyzed as shown in Fig. 4(a). The geometrical structures of the inlet and outlet tubes and the flow manifolds are the same as those of the MPFAR. Only the structure of the micro-channels with catalyst coated on is different with the MPFAR. To reduce the computing time, one micro-channel of the micro-channel reactor is selected as the simulation domain in this study. The schematic diagram of the micro-channel is shown in Fig. 4(b). The channel width, length, fin thickness and height are 800 μm, 18 mm, 1 mm, and 1.2 mm, respectively, which are similar with those of the MPFAR, and the micro-channel also includes the catalyst layer and flow channel for comparisons.

3.2. Scale analysis

Considering the heat and mass transfer of gaseous reactants in the micro-reactor, the micro flow modeling should be checked whether the continuum model or the rarefied model is to be used. This depends on the value of Knudsen number $K_n = \lambda/D_c$ [30], where

Table 1
Geometrical parameters of the MPFAR.

Micro-channel length L (m)	1.8×10^{-2}
Micro-channel width W (m)	2.1×10^{-2}
Micro-channel height H (m)	1.2×10^{-3}
Micro-pin-fin arrays height h (m)	1.0×10^{-3}
Micro-pin fin diameter d (m)	1.0×10^{-3}
Transverse center-to-center distance S_T (m)	1.8×10^{-3}
Longitudinal center-to-center distance S_D (m)	1.8×10^{-3}
Flow manifold length L_M (m)	1.0×10^{-2}

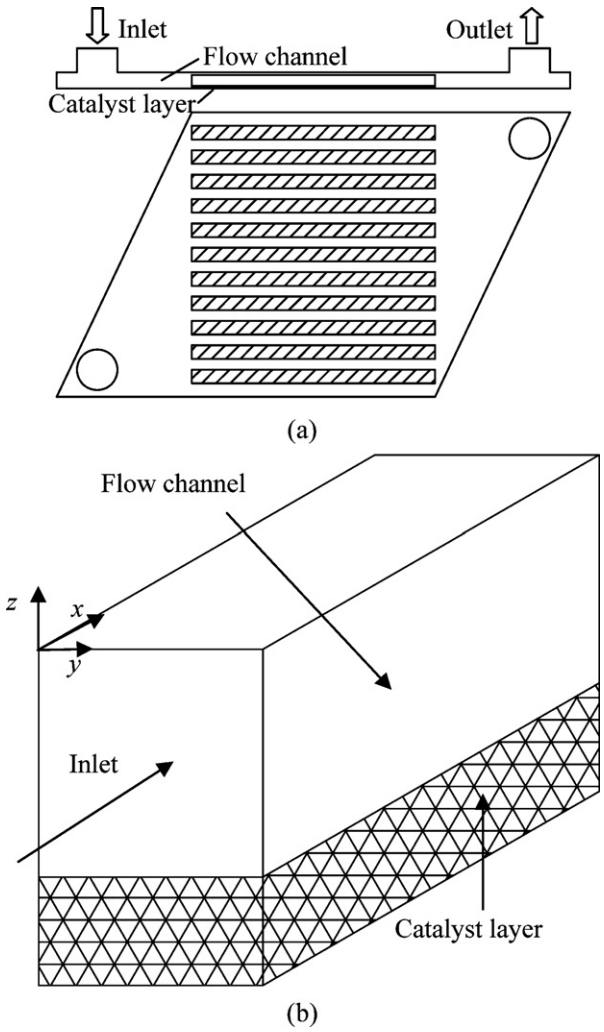

Fig. 4. Schematic diagram of a micro-channel reactor: (a) 2-D structure diagram of the micro-channel reactor; (b) 3-D structure diagram of a micro-channel.

λ and D_c are the mean free path for a gas molecule and the characteristic length, respectively. If $K_n < 10^{-3}$, the continuum model is suitable. K_n can be calculated as follows:

Assuming all the fluid is steam in the micro-reactor, and the minimum values of D_c in this study is 0.855 mm, then the maximum mean free path is

$$\lambda = \frac{f}{\sqrt{2}\pi\rho_g {d_g}^2} = 1.58 \times 10^{-7}(m)$$

The maximum value of K_n is

$$K_n = \frac{\lambda}{D_c} = 1.85 \times 10^{-4} < 10^{-3}$$

On the other hand, assuming all the fluid is methanol gas in the micro-reactor, thus, the maximum mean free path is

$$\lambda = \frac{f}{\sqrt{2}\pi\rho_g {d_g}^2} = 1.39 \times 10^{-7}(m)$$

The maximum value of K_n is

$$K_n = \frac{\lambda}{D_c} = 1.62 \times 10^{-4} < 10^{-3}$$

Because all the values of K_n are less than 10^{-3}, indicating that the N–S equations is suitable to analyze the heat and mass transfer in the MPFAR and the micro-channel reactor.

3.3. Modeling description

The reaction schemes for methanol steam reforming with the catalyst of $Cu/Zn_2O_3/AL_2O_3$ used in this study are as follows [31]:

$$CH_3OH + H_2O = 3H_2 + CO_2 \quad (1)$$

$$H_2 + CO_2 = CO + H_2O \quad (2)$$

Its species equation can be expressed as:

$$\rho\left(u\frac{\partial Y_s}{\partial x} + v\frac{\partial Y_s}{\partial y} + w\frac{\partial Y_s}{\partial z}\right) = D_{eff}\,\rho\left(\frac{\partial^2 Y_s}{\partial x^2} + \frac{\partial^2 Y_s}{\partial y^2} + \frac{\partial^2 Y_s}{\partial z^2}\right) + R_s \quad (3)$$

where ρ is the density of fluid; u, v, w are velocity components in the x, y and z direction, respectively; x, y, z are Cartesian coordinates; Y_s is the mass fraction of the sth species, including CH_3OH, H_2O, H_2, CO and CO_2; D_{eff} is the mass diffusion coefficient, which can be expressed as $D_{eff} = \varepsilon^{\gamma} D$ [20], where ε is the porosity. The values of D_{eff} are 0.38 and 1 in the flow channel and the catalyst layer, respectively; γ is set as 1 in this study; R_s is the species source term for the reforming reaction. For the flow channel, R_s is zero as no reaction occurs, while for the catalyst layer, R_s can be expressed as

$$R_s = M_{ws}(R_{SR} + R_{rWGS})(\lambda'' - \lambda') \quad (4)$$

where M_{ws} is the molecular weight of the species s, R_{SR} is the reaction rate of the steam reforming reaction, R_{rWGS} is the reaction rate of the reverse water-gas shift reaction (rWGS). Based on reaction schemes mentioned above, the reaction rate equations are [32]

$$R_{SR} = k_1 P_{CH_3OH}^{m} P_{H_2O}^{n}, \quad m = 0.6, n = 0.4 \quad (5)$$

$$R_{rWGS} = k_2 P_{CO_2} P_{H_2} - k_{-2} P_{CO} P_{H_2O} \quad (6)$$

where P_s is the partial pressure of species s; k_1 is the rate constant of the steam reforming reaction, k_2 and k_{-2} is the forward and backward rate of the reversal water-gas shift reaction.

The cross-section area of the reactor and the gas velocity analyzed in this study is small, so the value of the Reynolds number is small and the Mach number is less than 0.4. Consequently, the flow can be supposed as laminar and incompressible. Considering the steady state, the three-dimensional continuity equation is [23]

$$\rho\left(\frac{\partial u}{\partial x} + \frac{\partial v}{\partial y} + \frac{\partial w}{\partial z}\right) = 0 \quad (7)$$

The momentum equations of the fluid in the micro-reactor are as follows [23]:

X-momentum equation,

$$\rho\left(u\frac{\partial u}{\partial x} + v\frac{\partial u}{\partial y} + w\frac{\partial u}{\partial z}\right) = -\frac{\partial p}{\partial x} + \mu\left(\frac{\partial^2 u}{\partial x^2} + \frac{\partial^2 u}{\partial y^2} + \frac{\partial^2 u}{\partial z^2}\right) + S_u \quad (8)$$

Y-momentum equation,

$$\rho\left(u\frac{\partial v}{\partial x} + v\frac{\partial v}{\partial y} + w\frac{\partial v}{\partial z}\right) = -\frac{\partial p}{\partial x} + \mu\left(\frac{\partial^2 v}{\partial x^2} + \frac{\partial^2 v}{\partial y^2} + \frac{\partial^2 v}{\partial z^2}\right) + S_v \quad (9)$$

Z-momentum equation,

$$\rho\left(u\frac{\partial w}{\partial x} + v\frac{\partial w}{\partial y} + w\frac{\partial w}{\partial z}\right) = -\frac{\partial p}{\partial x} + \mu\left(\frac{\partial^2 w}{\partial x^2} + \frac{\partial^2 w}{\partial y^2} + \frac{\partial^2 w}{\partial z^2}\right) + S_w \quad (10)$$

where p is the pressure of fluid; μ is the dynamical viscosity of fluid; S_u, S_v, S_w are the sources terms produced by the porous structure of catalyst, therefore, in flow channel S_u, S_v, S_w are all zero, while in the catalyst layer, their representations are depicted in Ref. [33].

Table 2
Thermo-physical parameters [34].

Species	C_p (J kg^{-1} K^{-1})	κ (W m^{-1} K^{-1})	μ (kg m^{-1} s^{-1})
CO_2	Piecewise-linear	0.0323	2.65×10^{-5}
CO	Piecewise-linear	0.0386	2.84×10^{-5}
H_2	Polynomial	Polynomial	Polynomial
CH_3OH	Piecewise-linear	0.0351	1.88×10^{-5}
H_2O	Polynomial	Polynomial	Polynomial

Because the reaction temperature of SMR is relatively low (less than 553 K), the thermal radiation and conduction in the gas phase can be negligible in the calculation, so the energy equation is

$$\rho\left(u\frac{\partial T}{\partial x} + v\frac{\partial T}{\partial y} + w\frac{\partial T}{\partial z}\right) = \frac{\kappa}{C_p}\left(\frac{\partial^2 T}{\partial x^2} + \frac{\partial^2 T}{\partial y^2} + \frac{\partial^2 T}{\partial z^2}\right) + R_r + \varphi \quad (11)$$

where C_p is the specific heat in a constant pressure; T is the fluid temperature; κ is the fluid heat conductivity; R_r is the energy source term for reforming reaction; φ is the fluid viscous dissipation term and it can be expressed as

$$\varphi = \mu\left[2\left(\frac{\partial u}{\partial x} + \frac{\partial v}{\partial y} + \frac{\partial w}{\partial z}\right)^2 + \left(\frac{\partial u}{\partial y} + \frac{\partial v}{\partial z} + \frac{\partial w}{\partial x}\right)^2\right] \quad (12)$$

The boundary conditions of the micro-reactor and the microchannel need to be specified. For comparison, the boundary conditions of the two reactors keep consistent. The boundary conditions used in this study are similar to Ref. [22], including those at the inlet, outlet, wall and the interfaces between the flow channel and the catalyst layer. The detailed boundary conditions are as follows:

(1) The boundary conditions for the inlets at the flow channel and the catalyst layer: The inlet flow velocity, the inlet gas composition and the inlet temperature are constant.
(2) The boundary conditions for outlets at the flow channel and the catalyst layer: There is fully developed flow; the gauge pressure at outlet is zero.
(3) The boundary conditions for the interface between the heated wall and the catalyst layers: The velocities and the concentration gradient are assumed to be zero, and the temperature is assumed to be equal to the constant wall temperature.
(4) The boundary conditions for the interface between the flow channel and the catalyst layer: The temperature, velocities, species concentration and species flux are continuous.
(5) The boundary conditions for the walls except heated wall: The walls are assumed to be adiabatic.

4. Numerical studies and discussion

The equations mentioned above in the study were solved by employing a finite volume scheme with the simulation domain divided into a lot of cells, which were used as control volumes. The equations are numerically integrated over each control volumes. All equations were numerically solved by using the commercial fluid dynamics program, ANSYS FLUENT 12.1.2 (2009, ANSYS, Inc.). The SIMPLE algorithm was used to solve the conversion-diffusion equations.

The five species including CO_2, CO, H_2, H_2O and CH_3OH are considered as ideal gas. Their thermo-physical parameters are shown in Table 2. The density of gas mixture is assumed as non-compressive ideal gas. The corresponding thermo-physical parameters obey the mass-weight mixing law.

To analyze the performance of the micro-reactor, the temperature and velocity distribution in the micro-reactor are investigated firstly in this study. For calculation, the inlet temperature of reagents keeps constant to 473 K. Due to the continuum model used in the simulation, the distance between the two adjacent micro-pin-fins cannot be smaller than several tens of micrometers. Also for the laminar assumption, the occurrence of the turbulence should be avoided in the flow when the parameter Re is several hundred, so the maximum inlet velocity calculated by the parameter Re in this calculation should be lower than 3.367 m s^{-1} for the accuracy of the simulation. Therefore, the effect of the SC^{-1} molar ratios (1.0, 1.1, 1.2, 1.3, 1.4, 1.5, 1.6), reaction temperatures (493.15 K, 523.15 K, 553.15 K, 593.15 K) and contact times (0.031 s, 0.0413s, 0.062 s, 0.0815s, 0.12 s, 0.16 s, 0.2 s, 0.24 s) on the methanol conversion and the species molar fraction are also investigated. The contact time can be defined as $\tau = V_{cat}/V_r$, where V_{cat}, V_r are the volume of the catalyst layer and the volumetric flow rate of gaseous methanol and water, respectively. The methanol conversion can be calculated as $\eta_M(\%) = (C_i - C_{out})/C_i \times 100$, where C_i and C_{out} are the inlet and outlet CH_3OH molar concentration, respectively. In addition, the methanol conversion in the MPFAR is compared with a micro-channel reactor under the same operation condition.

To investigate the effect of the grids density on the simulated results, the grids independence was examined at the beginning of the simulation. Three grid configurations were evaluated for the micro-reactor and the micro-channel. The numbers of the grids are 149,270, 592,706, and 1,178,480, and the numbers of the grids of the micro-channel are 8,640, 38,880, and 69,120. The influence of the grids on the methanol conversion is shown in Table 3. From Table 3, it can be found that the both three values of methanol conversion for the two reactors are almost consistent, so the grid number of 149,270 and 8,640 are chosen for the MPFAR and the micro-channel in this study to reduce the computation time, respectively. The normalized residuals of the variable were calculated and the convergence criterions for the normalized residuals for each variable were restricted to less than 5×10^{-6}. From calculation results, the minimum value among the calculated methanol and CO molar fraction is larger than 10^{-3}, therefore, the error ranges of each variable is within ±1%, whose influence on the results is very small and can be neglected.

4.1. Distribution of the temperature, velocity and M_i in the MPFAR

Fig. 5 shows the temperature distribution in the micro-reactor at the plane of $z = 0.5$ mm when the reaction temperature is 553.15 K. From the reactor inlet to outlet, the temperature increases from 552 K to 553.15 K. The temperature keeps constant in the inlet flow manifold since there is no catalyst in that region. Because of the endothermic characteristic of the steam reforming reaction, the temperature in the inlet portion of micro-pin-fin arrays is lower than the wall temperature. But from Fig. 5, it can be found that the temperature gradient is only about 1 K in the reaction region. The lower temperature gradient can avoid the appearance of "cool point" [35] and will provide a great reaction environment for catalyst. Fig. 6 shows the velocity distribution under the same condition as Fig. 5. From Fig. 6, it can be found that the velocity distribution is uniform along the flow direction of reagents in micro-pin-fin arrays, which can enhance the reaction performance of SMR effectively. The velocity around the micro-pin-fins is small, meaning that the mass diffusion is the key factor in transporting reagents to catalyst. The fluid velocity at the outlet of the MPFAR is about two times than that at the inlet which agrees well with the reaction scheme of SMR. The velocity distribution in other planes of direction z is also uniform as shown in Fig. 6, though the velocity is different.

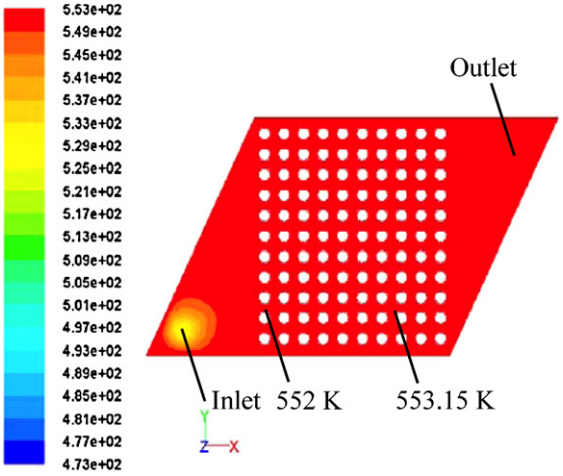

Fig. 5. The simulated temperature distribution of the MPFAR in the plane of $z = 0.5$ mm under the condition that the reaction temperature, the SC^{-1} molar ratio and the contact time are 553.15 K, 1.2 and 0.041 s, respectively.

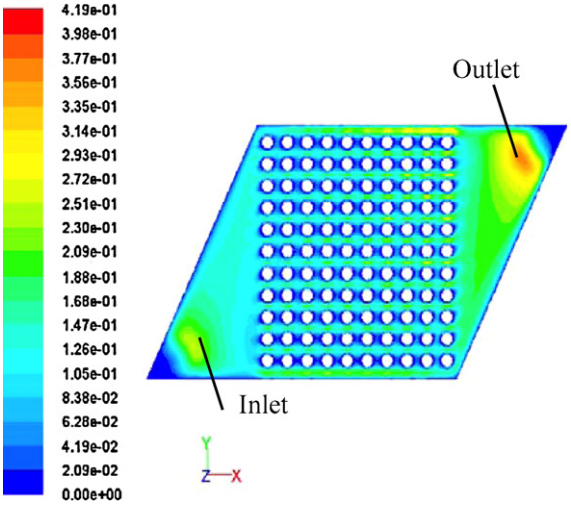

Fig. 6. The simulated velocity distribution of the MPFAR in the plane of $z = 0.5$ mm under the same condition as Fig. 5.

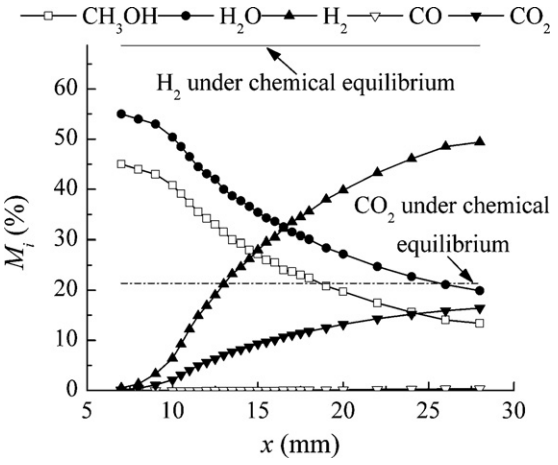

Fig. 7. The simulated mean molar fraction distribution of various species along x direction in the MPFAR under the same condition as Fig. 5.

Table 3
Methanol conversion for the different grids under the same conditions.

	Micro-channel reactor			MPFAR		
Grids	149,270	592,706	1,178,480	8,640	38,880	69,120
η_M (%)	82.8227	82.8163	82.8295	90.5009	90.6995	90.8345

Fig. 7 depicts the molar fraction distribution of the different species in the MPFAR. Along the *x* direction (flow direction) of the reagents, the CH_3OH and H_2O molar fractions decrease, while the H_2, CO_2, and CO molar fractions increase. As it is known that the ratio of the molar fraction between H_2 and CO_2 is equal to 3 if the steam reforming reaction occurs only, but the ratio is not exactly equal to 3 due to the rWGS in SMR. From Fig. 7, the ratio of the molar fraction between H_2 and CO_2 is approximately equal to 3, which means that the steam reforming reaction is dominating in the MPFAR. In addition, it is also found that the CH_3OH molar fraction decreases more steeply at the inlet, owing to a bigger reaction rate in the inlet region. The thermodynamic equilibrium compositions of H_2 and CO_2 are also depicted in Fig. 7. It can be found that H_2 molar fraction under equilibrium condition is 68.72, which is higher than the H_2 molar fraction at outlet. This result indicates that the methanol steam reforming is not under thermodynamic equilibrium condition.

4.2. The effect of Tr, τ, SC^{-1} molar ratio on η_M and M_{CO}

Fig. 8(a) shows the methanol conversion at different reaction temperatures and contact times when the SC^{-1} molar ratio is 1.2. From Fig. 8(a), it can be found that the methanol conversion increases with the increase of the reaction temperature and the contact time. However, a careful analysis of Fig. 8 reveals that the reaction temperature plays a key role on SMR reaction. When the temperature is 493.15 K, the methanol conversion is still less than 60% even the contact time is as long as 0.24 s, while when the temperature is 593.15 K, the methanol conversion in the MPFAR is more than 80% at any contact time. Furthermore, the methanol conversion under thermodynamic equilibrium condition when the reaction temperature is 593.15 K is also depicted in Fig. 8. It can be found that the methanol steam reforming reaction approaches to thermodynamic equilibrium when the methanol conversion approaches to 100%. The CO molar fraction in the reformate gas at the outlet of the micro-reactor under different reaction temperatures and contact times is shown in Fig. 8(b). The CO molar fraction increases more quickly at a higher reaction temperature with the increase of the contact time. This means that the effect of the contact time on the CO molar fraction is large at a higher reaction temperature.

Fig. 9 depicts the effect of the SC^{-1} molar ratio on the methanol conversion and the CO molar fraction at different reaction temperatures when the contact time is 0.041 s. From Fig. 9(a), it can be found that though the temperature plays a key role on the methanol conversion, the influence of the SC^{-1} molar ratio on the methanol conversion is similar at various reaction temperatures. This means that the SC^{-1} molar ratio and the reaction temperature independently influence the methanol conversion. However, the change rates of the CO molar fraction at low and high temperature are small and large, respectively. Also, with the increase of the SC^{-1} molar ratio, the methanol conversion increases, while the CO molar fraction decreases. This can be easily explained by Le Chatelier's principle. Excess steam in the reagents enhances the SMR and inhibits the rWGS. However, the increase of the SC^{-1} molar ratio needs the SMR system to supply more energy for gasifying the reagents, making the system less efficient.

4.3. Comparison with a micro-channel reactor

Based on the model presented in Section 3.3, the performance comparison with a micro-channel reactor is conducted. For comparison, the flow rates at the inlet tubes of the two reactors are consistent, so the inlet velocities of the two simulation domains are different due to their different inlet dimensions. Fig. 10 shows the methanol conversion at different inlet flow rates and reaction temperatures when the SC^{-1} molar ratio is 1.2. Fig. 10 reveals that with the increase of the inlet flow rate and the reaction temperature, the methanol conversion in the micro-channel reactor increases. The comparisons between the MPFAR and the micro-channel reactor at the same catalyst thickness (100 μm) are made in Fig. 10. It is found that under the same reactor temperature and the inlet flow rate, the methanol conversion in the MPFAR is much higher than that in the micro-channel reactor. This is because the specific surface area of the MPFAR (Ca. 2634.9 $m^2\ m^{-3}$) is larger than the micro-channel reactor (Ca. 1320.6 $m^2\ m^{-3}$), which makes more catalyst mounted on the catalyst support.

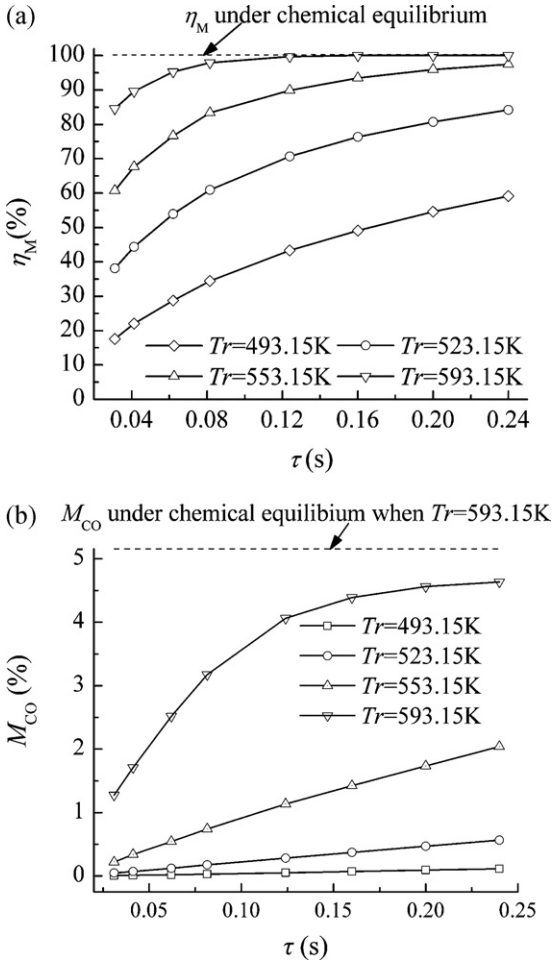

Fig. 8. The effect of the contact time and reaction temperature with the SC^{-1} molar ratio of 1.2 on: (a) methanol conversion and (b) CO molar fraction in the reformate gas at the outlet.

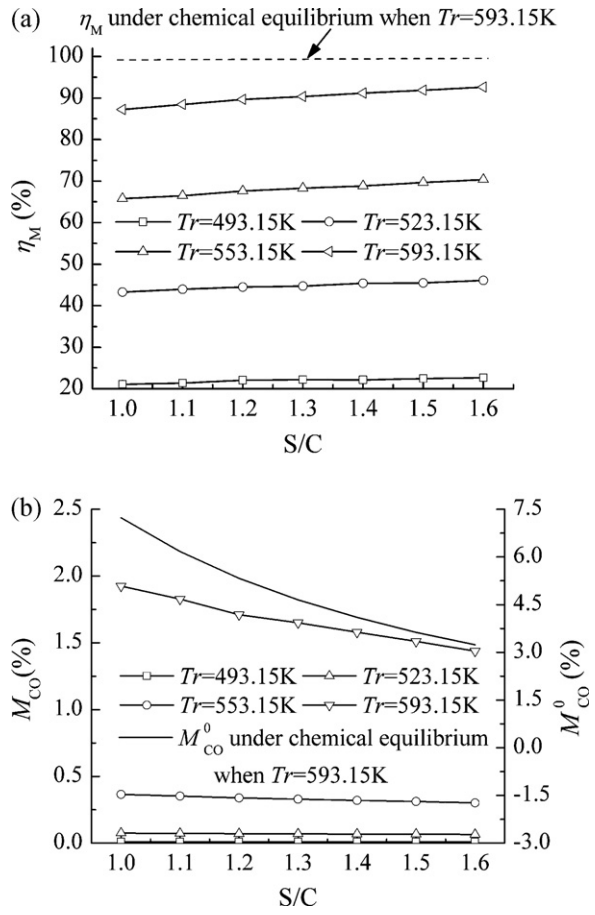

Fig. 9. The effect of the SC^{-1} molar ratio with the contact time of 0.041 s on: (a) methanol conversion and (b) CO molar fraction in the reformate gas at the outlet.

When the catalyst thickness is 418.7 μm in the micro-channel reactor and 100 μm in the MPFAR, the catalyst weight in the two micro-reactors is equal. In this case, it is found from Fig. 10 that the methanol conversion in the former is higher than that in the latter. This result demonstrates that micro-pin-fin arrays can enhance

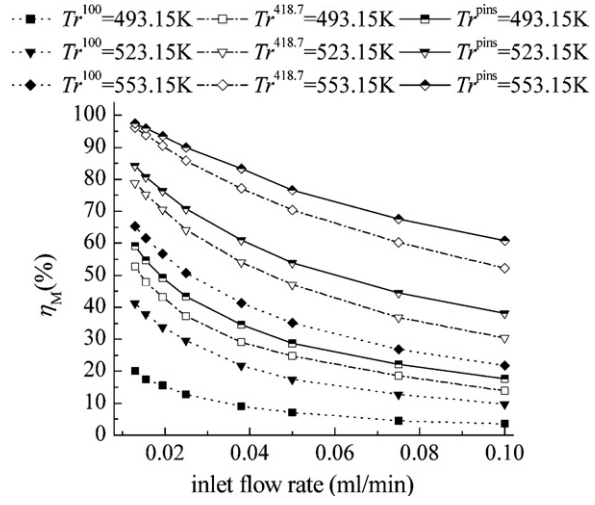

Fig. 10. Comparisons of the methanol conversion between the MPFAR and a micro-channel reactor in two cases: the catalyst thickness is equal and the catalyst weight is equal (Tr^{pins}, Tr^{100} and $Tr^{418.7}$ represent the reaction temperature of the MPFAR, the micro-channel reactor with the catalyst thickness of 100 μm and the micro-channel reactor with the catalyst thickness of 418.7 μm, respectively).

the heat and mass transfer. The higher contact area of the MPFAR reduces the thickness of catalyst layer, making the preparation easy.

5. Experimental validation

For evaluating the performance of the MPFAR, optimizing operation conditions and verifying the reliability of the numerical simulation, a series of experiments were conducted. The contact time, the reaction temperature and the SC^{-1} molar ratio were varying in the range of 0.031-0.12 s (in the room temperature), 493-553 K, and 1.0-1.5, respectively. The experimental results were compared with the simulated ones obtained in Section 4, and the detail processes are as follows.

5.1. The reaction system and experimental setup

Fig. 11 denotes the schematic diagram of the reaction system for hydrogen production via SMR. The reaction system consisted of three subsystems including a reagent feeding unit, a MPFAR, a reformate gas treatment and analysis unit. In the reagent feeding unit, a flask was used to store the mixture of methanol and water, a steel cylinder was employed to contain the gas mixture of H_2 and N_2 with 5 vol.% H_2, and an evaporator was used to generate gaseous reactant for the MPFAR. As for the MPFAR, it is composed of four cartridge heaters with small diameter, two J-type thermocouples for the temperature control. In the reformate gas treatment and analysis unit, a condenser, a gas–water separator and a dryer were used to treat the reformate gas. The gas chromatographer (Agilent 7890A) with a TCD detector and a flow meter were used to analyze the product gases.

5.2. Experimental procedures

The experimental procedures for the performance testing of the fabricated MPFAR for hydrogen production are sketched in Fig. 11. In this study, $Cu/ZnO/Al_2O_3$ catalyst was used for hydrogen production. The catalyst was reduced in the N_2/H_2 gas mixture with 5 vol.% H_2 under the flow rate of 100 sccm at 523 K for 6 h. The flow rate was controlled by a mass flow meter in conjunction with LABVIEW software. After reduction, N_2 was fed into the reactor for about 10 min at a flow rate of 50 sccm to remove the residual gases. Then, the reagents were fed into the evaporator and the micro-reactor with a specified flow rate controlled by a spring pump. A thermocouple was mounted at the outlet of the evaporator, controlling the inlet temperature of the micro-reactor. For consequent analysis of the reformate gas, the residual methanol and water were removed by a condenser, a gas-liquid separator and a dryer. Following the treatment of the reformate gas, the volumetric flow rate of the outlet gases was detected by a flow meter with the unit of sccm. The volumetric fraction of the different gas species was detected by a gas chromatographer with a TCD detector. According to the research work of Choi et al. [36], when the feed contains 43 mol. % water or greater, no by-products such as methane and methyl are detected in the temperature range of 473–573 K. Therefore, the by-products were neglected in this study due to the similar reaction conditions. In order to ensure the experimental quality, the gas chromatographer was calibrated by the standard gas. The thermocouples and the flow meter were also calibrated accurately before experiments. In addition, the reaction system was leak tested by sending N_2 with a fixed volumetric flow rate into the reaction system for the SMR reaction followed by measuring the flow rate at the outlet of the dryer.

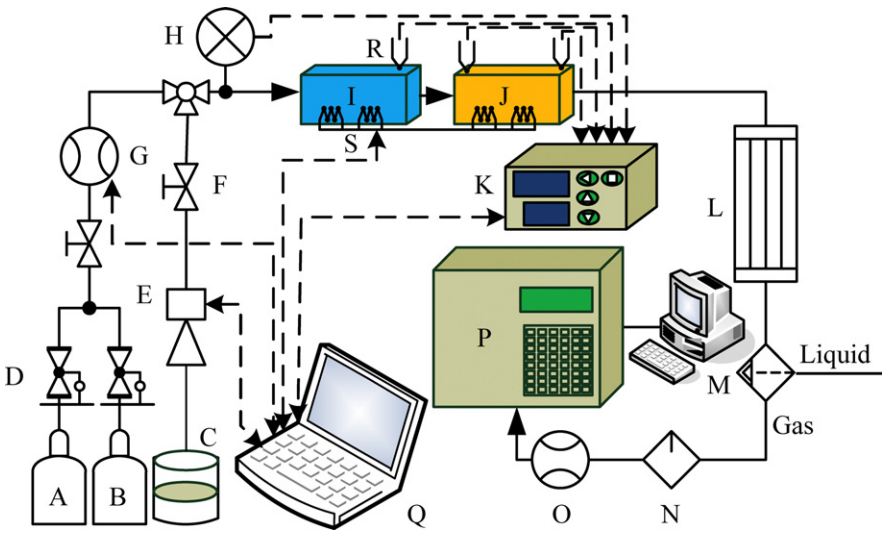

Fig. 11. A schematic diagram of the reaction system (A: N_2/H_2 mixture; B: N_2; C: methanol and water mixture; D: pressure relief valve; E: pump; F: shut off valve; G: mass flow meter; H: pressure meter; I: evaporator; J: MPFAR; K: temperature display device; L: condenser; M: gas-liquid separator; N: drier; O: flow meter; P: laptop computer; Q: gas chromatographer; R: thermocouples; S: cartridge heaters).

5.3. Experimental results and discussion

In this study, different contact times are selected for comparing the experimental results with the simulated ones. Fig. 12 shows the methanol conversion, the CO molar fraction at the outlet under various contact times and reaction temperatures when the $S\,C^{-1}$ molar ratio is 1.2. It can be found that with the increase of the contact time, the methanol conversion increases, but the inlet flow decreases because of the fixed volume of the micro-reactor. Therefore, the hydrogen yields of the MPFAR decreases from 0.00498 mol s^{-1} to 0.00180 mol s^{-1} with the reaction temperature of 553.15 K when the contact time increases from 0.031 s to 0.12 s. As the contact time is 0.12 s, the methanol conversion reaches to 87.5%. Fig. 12 also depicts the CO molar fraction under various contact times when the reaction temperature is 523 K. The contact time changes from 0.031 s to 0.12 s, the CO molar fraction in the reformate gas increases from 0.13 to 0.26. This result shows that CO is the consecutive product in the SMR process and this also agrees well with the research work performed by Men et al. [8].

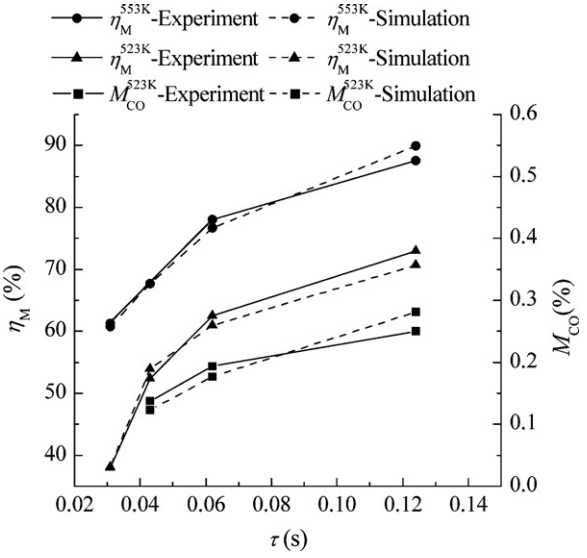

Fig. 12. Comparisons of the simulated methanol conversion and CO molar fraction with the experimental results.

Fig. 13 depicts the methanol conversion and the species fraction at different temperatures when the contact time and the $S\,C^{-1}$ molar ratio are 0.031 s and 1.2, respectively. With the increase of the reaction temperature, the methanol conversion and the CO molar fraction in the reformate gas increase. The CO molar fraction demonstrated from Fig. 13 is less than 1% in the reformate gas. Simulated results of the methanol conversion are also indicated in Fig. 13, and the reasonable agreement with each other can be found.

Fig. 14 depicts the methanol conversion and the species molar fraction in the reformate gas at various $S\,C^{-1}$ molar ratios when the reaction temperature and the contact time are 523 K and 0.031 s, respectively. From Fig. 14(a), it can be found that with the increase of the $S\,C^{-1}$ molar ratio, the methanol conversion increases, but the increase of the H_2 yields is not consistent with the methanol conversion. This is because the increase of the $S\,C^{-1}$ molar ratio results in the decrease of the methanol molar flow rate with the same volumetric flow rate. The simulated results about the methanol conversion and the species fraction are also depicted in Fig. 14. It can be found that the maximum error of the methanol conversion

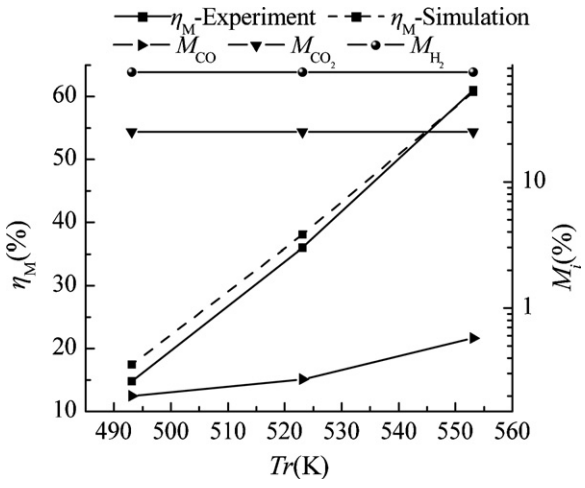

Fig. 13. Comparison of the methanol conversion between the experimental results and the simulated ones, and the experimental results of the species molar fractions under the condition that the $S\,C^{-1}$ molar ratio and contact time are 1.2 and 0.031 s, respectively.

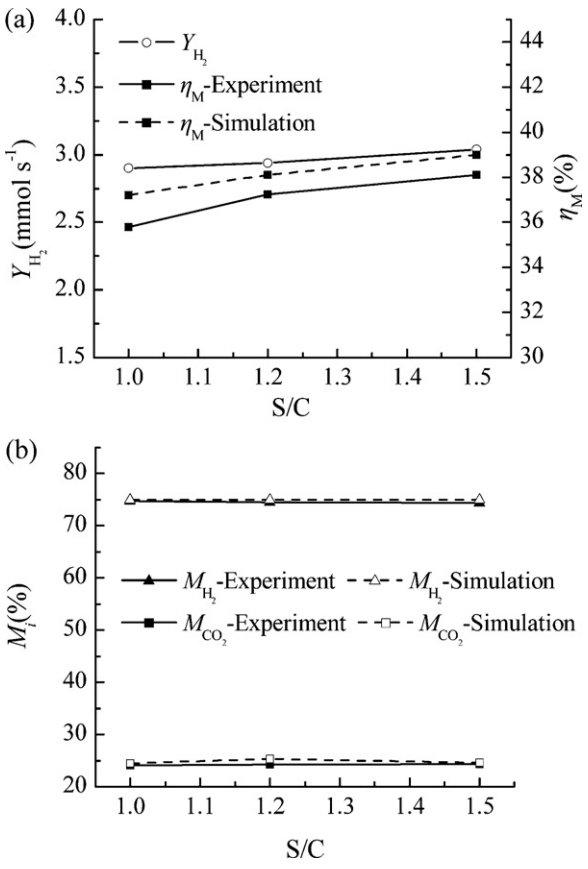

Fig. 14. Methanol conversion, H_2 yields and species molar fractions at various S C^{-1} molar ratios under the condition that the temperature reaction and the contact time are 523 K and 0.031 s, respectively: (a) comparison of the methanol conversion between the experimental results and the simulated ones, and the experimental results of H_2 yields; (b) comparison of the species molar fractions between the simulated results and the experimental ones.

between the experimental results and the simulated ones is less than 6%, and the small discrepancy shows that the simulated results about the methanol conversion are reasonably consistent with the experimental ones. It is also found that for H_2 and CO_2, the calculated results agree well with the experimental measurements.

6. Conclusions

A novel MPFAR is developed and fabricated using micro thixoforming technology in this study to enhance the performance of the micro-reactor for hydrogen production and reduce the fabrication cost of the catalyst support. A three-dimensional model in the numerical analysis is adopted to investigate the heat and mass transfer in the MPFAR. Results demonstrate that the temperature and velocity distribution in the MPFAR developed in this study are uniform, which is beneficial for the SMR process. The methanol conversion as well as the CO molar fraction in the reformate gas at the outlet increases with the increase of the reaction temperature and the contact time. With the increase of the S C^{-1} molar ratio, the methanol conversion increases, while the CO molar fraction decreases. The comparisons between the MPFAR and the micro-channel reactor demonstrate that the former has better performance for hydrogen production. Series of experiments are also conducted to test the fabricated micro-reactor and it is found that the simulated results agree well with the experimental ones. Based on the experimental results, the methanol conversion in the MPFAR can reach to 87.5% with the H_2 molar fraction of about 75% which could provide enough hydrogen for fuel cell when the reaction temperature, the S C^{-1} molar ratio and the contact time are 553 K, 1.2 and 0.12 s, respectively.

The research works in this study would provide the theoretical basis for the continuum design, manufacture and optimization of the laminar MPFAR for hydrogen production by steam reforming of alcohol.

Acknowledgements

The authors would like to acknowledge the supports from National Natural Science Foundation of China (Grant Nos. 50930005, 51175460), Zhejiang Provincial Natural Science Foundation of China (Grant No. Z1090373), and Research Fund for the Doctoral Program of Higher Education of China (Grant No. 20110101110011).

References

[1] N. Zamel, X. Li, J. Power Sources 155 (2006) 297–310.
[2] J.C. Amphlett, R.F. Mann, R.D. Weir, Can. J. Chem. Eng. 66 (1988) 950–956.
[3] J.D. Holladay, J. Hu, D.L. King, Y. Wang, Catal. Today 139 (2009) 244–260.
[4] W. Cai, F. Wang, A. van Veen, C. Descorme, Y. Schuurman, W. Shen, et al., Int. J. Hydrogen Energy 35 (2010) 1152–1159.
[5] A. Casanovas, M. Domínguez, C. Ledesma, E. Lopez, J. Llorca, Catal. Today 143 (2009) 32–37.
[6] A. Casanovas, M.S. Gerons, F. Griffon, J. Llorca, Int. J. Hydrogen Energy 33 (2008) 1827–1833.
[7] S.R. Palo, Chem. Rev. 107 (2007) 3992–4021.
[8] Y. Men, G. Kolb, R. Zapf, D. Tiemann, M. Wichert, V. Hessel, et al., Int. J. Hydrogen Energy 33 (2008) 1374–1382.
[9] G. Kolb, V. Cominos, C. Hofmann, H. Löwe, G. Nikolaidis, R. Zapf, et al., Catal. Today 20 (2007) 2–20.
[10] K. Schubert, J. Brandner, M. Fichtner, G. Linder, U. Schygulla, A. Wenka, Microscale Thermophys. Eng. 5 (2001) 17–39.
[11] G.G. Park, D.J. Seo, S.H. Park, Y.G. Yoon, C.S. Kim, W.L. Yoon, Chem. Eng. J. 101 (2004) 87–92.
[12] A. Kunda, J.H. Jang, H.R. Lee, S.H. Kim, J.H. Gil, C.R. Jung, et al., J. Power Sources 162 (2006) 572–578.
[13] W. Zhou, Y. Tang, M.Q. Pan, X. Wei, H. Chen, J. Xiang, Int. J. Hydrogen Energy 34 (2009) 9745–9753.
[14] Y. Kawamura, N. Ogura, T. Yamamoto, A. Igarashi, Chem. Eng. Sci. 61 (2006) 1092–1101.
[15] A. Varesano, I. Guaglio, G. Saracco, P.L. Maffettone, Ind. Eng. Chem. Res. 44 (2005) 759–768.
[16] T. Kim, S. Kwon, J. Micromech. Microeng. 16 (2006) 1760–1768.
[17] J.S. Suh, M.T. Lee, R. Greif, C.P. Grigoropoulos, J. Power Sources 173 (2007) 458–466.
[18] F. Chen, M.H. Chang, C.Y. Kuo, C.Y. Hsueh, W.M. Yan, Energy Fuel 23 (2009) 5092–5098.
[19] J.S. Suh, M.T. Lee, R. Greif, C.P. Grigoropoulos, Int. J. Hydrogen Energy 34 (2009) 314–322.
[20] A. Karim, J. Bravo, D. Gorm, T. Conant, A. Datye, Catal. Today 110 (2005) 86–91.
[21] A. Fazeli, M. Behnam, Int. J. Hydrogen Energy 35 (2010) 9496–9503.
[22] C.Y. Hsueh, H.S. Chu, W.M. Yan, J. Power Sources 187 (2009) 535–543.
[23] C.Y. Hsueh, H.S. Chu, W.M. Yan, Appl. Energy 87 (2010) 3137–3147.
[24] O.J. Kwon, S.M. Hwang, J.G. Ahn, J.J. Kim, J. Power Sources 156 (2006) 253–259.
[25] P. Pfeifer, K. Schubert, M.A. Liauw, G. Emig, Appl. Catal. A 270 (2004) 165–175.
[26] K. Steinhoff, U. Weidig, J. Weikert, Steel Res. Int. 75 (2004) 611–619.
[27] G.Y. Kim, M. Koc, R. Mayor, J. Ni, T. ASME-J. Manuf. Sci. Eng. 129 (2007) 237–245.
[28] G.Y. Kim, R. Mayor, H. Kim, J. Ni, T. ASME-J. Manuf. Sci. Eng. 129 (2007) 246–251.
[29] H.H. Zhou, D.Q. Dei, Z.C. Chen, Adv. Mater. Res. 154 (2011) 907–912.
[30] X. Chen, Kinetic theory and its application in the study of the flow and heat transfer, Tsinghua Publishing House, Beijing, 1996, In Chinese.
[31] H. Purnama, T. Ressler, R.E. Jentoft, H. Soerijianto, R. Schlögl, R. Schomäcker, Appl. Catal. A 259 (2004) 83–94.
[32] L. Pan, S. Wang, Chem. Eng. J. 108 (2005) 51–58.
[33] S. Ergun, Chem. Eng. Prog. 48 (2006) 572–578.
[34] S. Fukahori, H. Koga, T. Kitaoka, M. Nakamura, H. Wariishi, Int. J. Hydrogen Energy 33 (2008) 1661–1670.
[35] A. Karim, J. Bravo, A. Datye, Appl. Catal. A 282 (2005) 101–109.
[36] Y. Choi, H.G. Stenger, Appl. Catal. B 38 (2002) 259–269.